

On-chip quantum interference between two silicon waveguide sources

J. W. Silverstone,^{1,*} D. Bonneau,^{1,*} K. Ohira,² N. Suzuki,² H. Yoshida,² N. Iizuka,² M. Ezaki,² R. H. Hadfield,³ V. Zwiller,⁴ G. D. Marshall,¹ J. G. Rarity,¹ J. L. O'Brien,¹ and M. G. Thompson^{1,†}

¹Centre for Quantum Photonics, H. H. Wills Physics Laboratory & Department of Electrical and Electronic Engineering, University of Bristol, Merchant Venturers Building, Woodland Road, Bristol, BS8 1UB, UK

²Corporate Research & Development Center, Toshiba Corporation, 1, Komukai Toshiba-cho, Saiwai-ku, Kawasaki 212-8582, Japan

³School of Engineering, University of Glasgow, Glasgow, G12 8QQ, UK

⁴Kavli Institute of Nanoscience, TU Delft, 2628CJ Delft, The Netherlands

Integrated quantum optics promises to enhance the scale and functionality of quantum technologies, and has become a leading platform for the development of complex and stable quantum photonic circuits. Here, we report path-entangled photon-pair generation from two distinct waveguide sources, the manipulation of these pairs, and their resulting high-visibility quantum interference, all on a single photonic chip. Degenerate and non-degenerate photon pairs were created via the spontaneous four-wave mixing process in the silicon-on-insulator waveguides of the device. We manipulated these pairs to exhibit on-chip quantum interference with visibility as high as $100.0 \pm 0.4\%$. Additionally, the device can serve as a two-spatial-mode source of photon-pairs: we measured Hong-Ou-Mandel interference, off-chip, with visibility up to $95 \pm 4\%$. Our results herald the next generation of monolithic quantum photonic circuits with integrated sources, and the new levels of complexity they will offer.

Scalable implementations of photonic quantum computation [1], simulation,[2] communication [3], and sensing [4], require the combination of three on-chip elements: dynamically reconfigurable photonic circuitry, single-photon sources, and detectors.[5, 6] To date, increasingly complex quantum photonic circuits,[7–9] sources,[10–13] and detectors[14] have been shown independently, but the integration of more than one of these elements has proven difficult. Focussing on source-circuit integrations, initial demonstrations have consisted of a photon-pair source with passive directional coupler elements, forming a quantum relay,[15] and a source of colour-segregated, polarisation-entangled photons, using an on-chip polarisation rotator.[16] To date, there have been no demonstrations of both quantum state generation and manipulation on a single chip. Moreover, no experiment has yet interfered photons from multiple on-chip sources.

We present a monolithic device comprising two spontaneous photon-pair sources, integrated within a tuneable Mach-Zehnder interferometer, capable of generating and manipulating path-entangled two-photon $N00N$ states. High-visibility on- and off-chip quantum interference is observed between these sources. We show how our device can be used as a photon pair source, to produce two-colour (non-degenerate) or same-colour (degenerate) photon pairs in two on-chip spatial modes, and we use off-chip Hong-Ou-Mandel-type (HOM) quantum interference to test the potential of this source.

To date, most quantum waveguide circuits have been fabricated from glass-based materials, which offer low propagation loss, a wide transparency window, and efficient coupling to optical fibre, but also limit device functionality and suffer from large circuit footprints. The

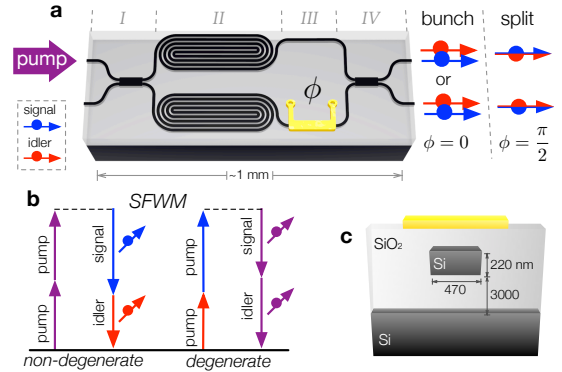


FIG. 1. **a.** Schematic operation of the device. A bright pump laser is coupled onto the silicon-on-insulator (SOI) chip using a lensed optical fibre and on-chip spot-size converters (not shown). The pump is distributed between two modes via a 2×2 multi-mode interference coupler (*I*), in each mode exciting the $\chi^{(3)}$ spontaneous four-wave mixing (SFWM) effect within a spiraled SOI waveguide (*II*), and producing signal-idler photon pairs in the two-photon entangled state $\frac{1}{2}(|20\rangle - |02\rangle)$. The pairs are thermo-optically phase shifted (ϕ , *III*), and interfered on a second coupler (*IV*) to yield either bunching or splitting over the two output modes, depending on ϕ . **b.** Energy diagrams of both types of SFWM, showing the time-reversal symmetry between the non-degenerate and degenerate processes. **c.** SOI waveguide cross-section, fabricated by standard CMOS processing techniques.

silicon-on-insulator photonics platform (SOI), recently developed for classical applications,[17, 18] has several advantages over glass-based systems, including a high component density, a strong $\chi^{(3)}$ optical nonlinearity, mature fabrication techniques, and compatibility with both 1550-nm telecom optics and CMOS electronics. As such, SOI quantum photonic circuits [19] and spontaneous photon-pair sources [10–12, 20, 21] have recently been

* Authors JWS and DB contributed equally to this work.

† mark.thompson@bristol.ac.uk

demonstrated.

Our SOI photonic device is presented in Fig. 1a. In the device are two photon-pair sources, each comprising a 5.2-mm-long spiraled silicon waveguide in which the $\chi^{(3)}$ spontaneous four-wave mixing (SFWM) process could occur (region *II*, Fig. 1a). SFWM creates a signal-idler photon pair by annihilating two photons from a bright pump beam (Fig. 1b). Non-degenerate pairs are created by a single-wavelength pump, while *degenerate* pairs require a dual-wavelength scheme.[22?] Pump distribution and single-photon interference were achieved using 2×2 multi-mode interference couplers (MMI), with reflectivity $\approx 50\%$, while a thermal phase-shifter modified the on-chip quantum and bright-light states. Off-chip wavelength-division multiplexers (WDM) were used to separate the signal, idler, and pump channels, before the photon pairs were finally measured by two superconducting single-photon detectors.

Evolution of the degenerate quantum and bright-light states proceeded, referring to regions (*I-IV*) of Fig. 1a, as follows. The bright pump was split by the first MMI (*I*) between the two sources (*II*). By operating in the weak pump regime (so that only one pair was likely to be generated), the simultaneous pumping of both sources generated a path-entangled $N00N$ state: $\frac{1}{\sqrt{2}}(|20\rangle - |02\rangle)$. The relative phase was then dynamically controlled via a thermal phase-shifter in one arm (*III*), which applied a ϕ shift to the bright-light pump and a 2ϕ shift to the entangled biphoton state: $\frac{1}{\sqrt{2}}(|20\rangle - e^{i2\phi}|02\rangle)$. Finally, the bright-light and biphoton states were interfered on the second MMI (*IV*) to yield Mach-Zehnder interference fringes for the bright pump, and half-period ($\frac{\lambda}{2}$ -like) fringes[23] for the photon pair, of the form

$$|\Psi_{\text{out}}\rangle = \cos \phi |\Psi_{\text{bunch}}\rangle + \sin \phi |\Psi_{\text{split}}\rangle. \quad (1)$$

Here, the $|\Psi_{\text{bunch}}\rangle$ state describes photons bunched together in either output mode *A* or *B*, and the $|\Psi_{\text{split}}\rangle$ state describes pair splitting, with one photon in each mode.[22] By considering the *degenerate* pair case, and specifically setting $\phi = 0$ or $\phi = \frac{\pi}{2}$, we can obtain either state at the output:

$$|\Psi_{\text{out}}\rangle = \begin{cases} |\Psi_{\text{bunch}}\rangle = \frac{1}{\sqrt{2}}(|20\rangle - |02\rangle), & \text{for } \phi = 0 \\ |\Psi_{\text{split}}\rangle = i|11\rangle, & \text{for } \phi = \frac{\pi}{2}. \end{cases} \quad (2)$$

When *non-degenerate* pairs are created, signal-idler exchange symmetry leads to identical quantum evolution and non-classical interference as eq. (2). The corresponding $|\Psi_{\text{bunch}}\rangle$ and $|\Psi_{\text{split}}\rangle$ states for non-degenerate SFWM are:

$$\begin{aligned} |\Psi_{\text{bunch}}\rangle &= \frac{1}{\sqrt{2}} \left(|1_s 1_i\rangle_A |0_s 0_i\rangle_B - |0_s 0_i\rangle_A |1_s 1_i\rangle_B \right) \\ |\Psi_{\text{split}}\rangle &= \frac{i}{\sqrt{2}} \left(|1_s 0_i\rangle_A |0_s 1_i\rangle_B + |0_s 1_i\rangle_A |1_s 0_i\rangle_B \right), \end{aligned} \quad (3)$$

where *s* and *i* indicate signal and idler wavelengths. We will show experimentally that these *non-degenerate* discretely colour-entangled[24, 25] states behave like *degenerate* pairs.

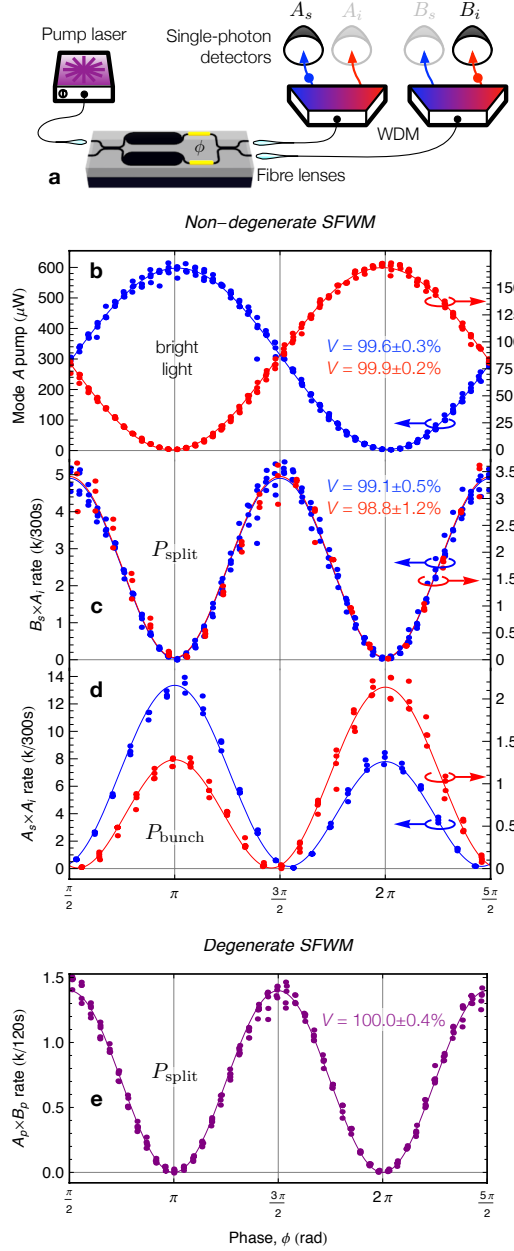


FIG. 2. On-chip quantum and classical interference measurements, varying the internal phase ϕ . Coincidence data have per-datum accidental coincidences subtracted. **a.** Apparatus, showing the coupling of light from a bright pump laser into the device, via fibre lenses, and the separation of signal (blue), idler (red), and pump (purple) wavelength channels using wavelength-division multiplexers (WDM). **b.** Transmission of the bright pump laser, showing classical interference. **c.** Measurement of signal-idler photon splitting between modes *A* and *B*. **d.** Measurement of signal-idler photon bunching, with signal and idler both in mode *A* or mode *B*. **e.** Photon splitting, like (b), but with monochromatic photon pairs, created with degenerate SFWM.

High-visibility quantum interference – non-classical interference between two photons on a beamsplitter – underpins all of photonic quantum information science and

technology. Quantum interference within our device was quantified by the splitting and bunching probabilities at the output, P_{split} and P_{bunch} , as the on-chip phase (ϕ) was varied; classical interference was observed in the transmission of the bright pump through the interferometer. We first manipulated the on-chip path entanglement of the two-colour (non-degenerate) pairs. The experimental apparatus is pictured in Fig. 2a, and detailed in Supplementary Section S1. Wavelength-division multiplexers (WDM) separated the monochromatic 1549.6-nm pump from the non-degenerate signal and idler photons (detuned by $\delta = 6.4$ nm) so that signal-idler coincidences and pump transmission could be measured at the same time. Detector coincidences $A_s \times B_i$ and $B_s \times A_i$ were measured for P_{split} , while $A_s \times A_i$ and $B_s \times B_i$ were measured for P_{bunch} . The rates of classical transmission, as well as P_{split} , and P_{bunch} are recorded in Figs. 2b, 2c, and 2d, respectively. In all cases, high-visibility interference was observed, and both the P_{split} and P_{bunch} two-photon fringes exhibited a phase-doubling compared to their classical counterparts – a signature of path-entangled two-photon states.

According to equation (1), the splitting rate should follow $P_{\text{split}} \propto \sin^2 \phi$ (curves, Fig. 2c). This model works well, with the data exhibiting a visibility $V \approx 99\%$ ($99.1 \pm 0.5\%$ for $A_i \times B_s$, and $98.8 \pm 1.2\%$ for $A_s \times B_i$), where we compute the visibility $V = (N_{\text{max}} - N_{\text{min}})/N_{\text{max}}$ from the maximum N_{max} and minimum N_{min} values of each fit. Meanwhile, for the bunching rate, eq. (1) predicts $P_{\text{bunch}} \propto \cos^2 \phi$, but, an asymmetric behaviour is observed, instead (Fig. 2d). This behaviour can be explained by considering spurious SFWM in the device's input and output (I/O) waveguides – which are identical in cross-section to the source waveguides (Fig. 1c). We calculate corrected bunching probabilities, P_{bunch}^A and P_{bunch}^B , at the two output modes A and B as,

$$\begin{aligned} P_{\text{bunch}}^B &= |(\Gamma_0 + \Gamma_{\text{I/O}}) \cos \phi \pm \Gamma_{\text{I/O}}|^2 \\ P_{\text{split}} &= |(\Gamma_0 + \Gamma_{\text{I/O}}) \sin \phi|^2 \end{aligned} \quad (4)$$

where Γ_0 is the base SFWM rate of the spiral sources, and $\Gamma_{\text{I/O}}$ quantifies the generation rate of spurious pairs inside the I/O waveguides (see Supplementary Section S2). Equation (4) fits the P_{bunch} data well (curves, Fig. 2c). We extracted the spurious pair rate $\Gamma_{\text{I/O}}^2$, and found that such pairs accounted for a small fraction of the total: $\Gamma_{\text{I/O}}^2/\Gamma_0^2 = 2.5\%$ for P_{bunch}^A , and 2.1% for P_{bunch}^B . Since SFWM efficiency scales quadratically with interaction length ($\Gamma^2 \propto L^2$, see Supplementary Section S2), we compared these ratios with the I/O-to-source waveguide-length ratio, squared, $L_{\text{I/O}}^2/L_0^2 = 2.0\%$, and found them to be similar. This gives us confidence that the P_{bunch} fringe asymmetry is caused by spurious pair generation in the I/O waveguides. The $\Gamma_{\text{I/O}}^2/\Gamma_0^2$ ratio is of considerable importance – it measures the amount of $|\Psi_{\text{bunch}}\rangle$ contamination when the device is configured to produce only $|\Psi_{\text{split}}\rangle$. It could be reduced, for example, by modifying the waveguide geometry outside the source regions,[11] or by moving to resonant sources.[12] In our experiment,

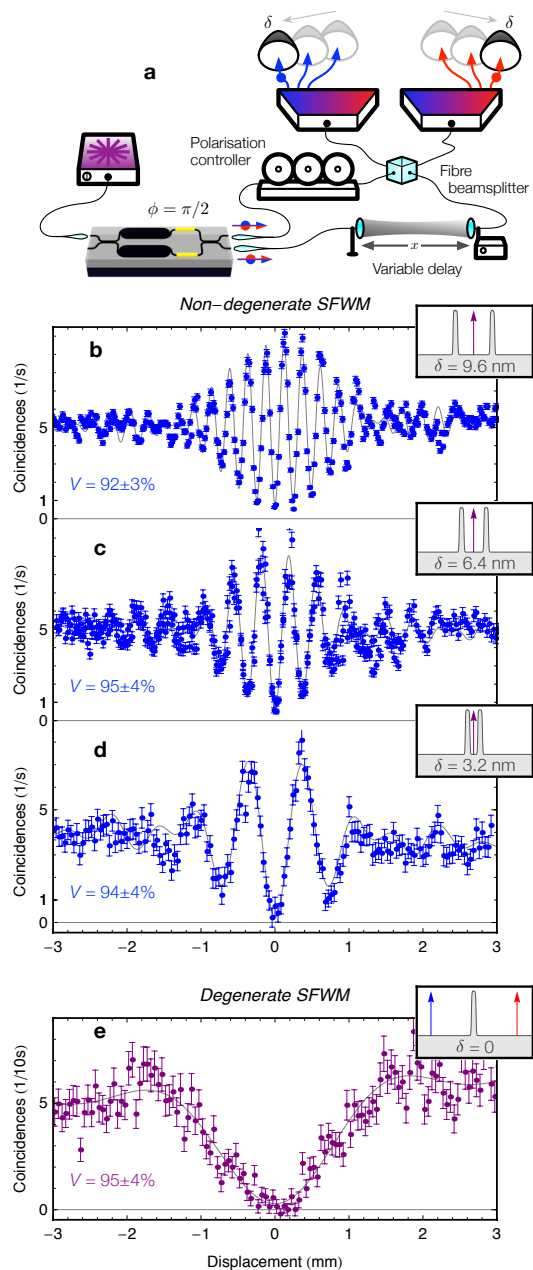


FIG. 3. Off-chip Hong-Ou-Mandel interference measurements for $|\Psi_{\text{split}}\rangle$. Beating within each fringe is explained by signal-idler detuning, δ , as plotted in insets to **b** - **e**. Coincidence data have per-datum accidental coincidences subtracted. Error bars are Poissonian, based on raw coincidences. **a**. Experimental schematic. Photon pairs in the $|\Psi_{\text{split}}\rangle$ state exit the chip, and one is delayed by displacement x , while the other is polarisation matched, then the pair is interfered on a beamsplitter. Two detectors measure coincidences at different signal-idler detunings δ . **b**. Detuning $\delta = 9.6$ nm (1200 GHz). **c**. Detuning $\delta = 6.4$ nm (800 GHz). **d**. Detuning $\delta = 3.2$ nm (400 GHz). **e**. Degenerate SFWM, no detuning.

spurious pairs limited the maximum observable off-chip quantum interference visibility to $V < 98\%$.

To show how our $|\Psi_{\text{split}}\rangle$ pairs could be used in an

external circuit, and to explore the implications of the colour entanglement described by eq. (3), we performed several off-chip Hong-Ou-Mandel-type quantum interference measurements,[26] for various values of the signal-idler detuning δ . The modified apparatus is pictured in Fig. 3a. We configured the device to generate $|\Psi_{\text{split}}\rangle$ at the chip output (by setting $\phi = \pi/2$), then sent one photon to a tunable delay line, and the other to a polarisation controller. Thus, the optical path and polarisation of the two photons could be precisely matched, and we could introduce distinguishability in the arrival time degree of freedom. The photon pair interfered on a fibre beamsplitter ($R = 50.2\%$), and we recorded coincidences while varying the arrival time (via the free-space displacement, x).

The phase-stable two-colour $|\Psi_{\text{split}}\rangle$ state yielded HOM interference fringes (Fig. 3b-d) which showed a beating between the non-degenerate signal and idler wavelengths (detuning δ).[25, 27] Due to the colour entanglement present in $|\Psi_{\text{split}}\rangle$ the filtered bi-photon spectrum has two lobes – one each from the signal- and idler-channel filters (insets Fig. 3b-d). Since the time-domain HOM interference pattern is effectively the Fourier transform of this spectrum, we can calculate the coincidence probability after the beamsplitter to be

$$P_{\text{HOM}} = \frac{1}{2} - \frac{V}{2} \cos\left(2\pi x \frac{\delta}{\lambda_p^2}\right) \text{sinc}\left(2\pi x \frac{w}{\lambda_p^2}\right), \quad (5)$$

where x is the delay displacement, λ_p is the pump wavelength, w is the WDM channel width, and δ is the signal-idler channel spacing. As we tuned $\delta \rightarrow 0$, the beat frequency decreased (Figs. 3b-d), as predicted by eq. (5). Off-chip HOM interference visibilities for each value of δ (subscripted) were measured: $V_{9.6\text{nm}} = 94 \pm 4\%$, $V_{6.4\text{nm}} = 95 \pm 4\%$, and $V_{3.2\text{nm}} = 92 \pm 3\%$. These results show how our device would perform as an on-chip two-photon source, based on high-fidelity on-chip entanglement.[25]

For a source that can drive general *multiphoton* experiments on-chip, however, we require uncorrelated[28] and *degenerate* pairs in discrete spatial modes, to allow arbitrary interference. Towards this goal, we produced degenerate photons via *degenerate* SFWM – the time-reversed version of the non-degenerate process – which requires a two-colour pump (Fig. 1b, see Supplementary Section S1 for apparatus details). Using degenerate SFWM, with a pump-signal detuning of 11.2 nm, we observed an on-chip quantum interference fringe with $V = 100.0 \pm 0.4$ (Fig. 2e), and measured off-chip HOM interference with $V = 95 \pm 4\%$. The HOM fringe shape corresponded to eq. (5) with $\delta = 0$.

Our results confirm that the on-chip-generated pairs from both degenerate and non-degenerate SFWM can yield high-visibility quantum interference, both on- and off-chip. Indeed, we observed on-chip visibilities higher than those measured off-chip. For this, two explanations exist: first, as mentioned, the off-chip visibility was limited by spurious pair generation in the I/O waveguides; and second, the HOM interference measurements

required both the on-chip phase, and the off-chip polarisation to be precisely set, and drifts in both parameters reduced the off-chip visibility. Regardless, the HOM visibilities were high, and we view the even higher *on-chip* visibilities as showing great promise for future high-fidelity[29] source-circuit integrations.

Despite these high measured visibilities, our on-chip sources were not bright. To extract the pair generation rate per source, we examined an isolated spiral waveguide: we measured a rate of 2.7 ± 0.4 kHz/nm/mW² for non-degenerate pairs, and a similar 2.5 ± 0.6 kHz/nm/mW² for degenerate pairs, with corresponding coincidence-to-accidental ratios of 290, and 45 (at 100 kHz). Brightness, however, is straightforward to improve, for example: by further engineering our spiral sources, improving the 10 dB facet loss, and optimising the spiral length; or by moving to resonant[12] or slow-light[21] SFWM enhancement.

Scalability is a key goal of any integrated quantum system. Bulk crystal spontaneous pair sources have been used successfully in the largest optical quantum information experiments to date – the production[30] and manipulation[31] of 8-photon entanglement. However, spontaneous sources can, in principle, be scaled beyond the limits of these post-selected arrangements by using active multiplexing and feed-forward techniques.[32, 33] We have shown that multiple on-chip SFWM sources can be made to interfere with high visibility, and so could one day form the backbone of these large-scale schemes. In the meantime, our device – a silicon-integrated source of photon-pairs in separate spatial modes – can serve as a drop-in replacement for current bulk SPDC sources. We look forward to the wealth of new and exciting applications that further on-chip integration will bring for optical quantum science.

METHODS

Optical apparatus. In the non-degenerate experiments, a narrow-linewidth tuneable laser (Tunics-Plus) was amplified using an erbium-doped fibre amplifier, then filtered to a 0.5-nm band using a four-port circulator (Opneti) with two cascaded fibre Bragg gratings (AOS GmbH), achieving > 50 dB of isolation from the signal and idler channels. We coupled the remaining ~ 20 mW to the chip using 2.0- μm mode-diameter lensed-fibres (OZ-Optics). From the output of the chip, each arm was first passed through another grating-circulator combination, in the reverse configuration, then a packaged silica 16×200 -GHz AWG (Opneti) separated the signal and idler, and suppressed the pump by a further > 90 dB. Single photons were counted by two free-running fibre-coupled superconducting nanowire single-photon detectors, operating at 5% (*A*) and 8% (*B*) efficiency, from which coincidence counting and timing was performed (PicoHarp 300), using a coincidence gating window of 650 ps.

In the degenerate experiments, a second pump laser

(Tunics-BT) was added, and both input and output filtering were accomplished solely using AWGs. This reduced filtering was sufficient, due to the increased spectral distance between the pump and single photon channels.

Electrical apparatus. An electrical probe (Cascade Microtech) was used to electrically interface between the chip and an ultra-low noise DC power supply (Agilent). We applied voltages up to 2.3 V to our thermo-optic phase modulator, for a maximum load of 36 mA. Similar devices exhibited fuse voltages around 2.7 V. Since steady-state temperature is proportional to dissipated power, we correlated electrical power with thermo-optic phase, with good results (Fig. 2b).

Fabrication. The silicon nanowire waveguides were fabricated from a silicon-on-insulator (SOI) wafer having a 220 nm slab thickness. The waveguides were designed to

be single-moded, having a width of 470 nm with a silicon dioxide upper cladding. I/O coupling was achieved using spot-size converters comprising a 300- μm -long inverse-taper with a 200-nm-wide tip beneath a $4 \times 4 \mu\text{m}^2$ polymer waveguide. Structures were defined by deep UV photolithography (248 nm) and dry etching.

ACKNOWLEDGEMENTS

The authors thank G. D. Marshall for useful discussions. This work was supported by EPSRC, ERC, the Centre for Nanoscience and Quantum Information (NSQI) and the European FP7 project QUANTIP. MGT acknowledges support from the Toshiba Research Fellowship scheme. JLOB acknowledges a Royal Society Wolfson Merit Award. RHH acknowledges a Royal Society University Research Fellowship.

-
- [1] J. L. O'Brien, *Science*, **318**, 1567 (2007).
- [2] A. Aspuru-Guzik and P. Walther, *Nat Phys*, **8**, 285 (2012), ISSN 1745-2473.
- [3] N. Gisin and R. Thew, *Nat Photon*, **1**, 165 (2007), ISSN 1749-4885.
- [4] A. Crespi, M. Lobino, J. C. F. Matthews, A. Politi, C. R. Neal, R. Ramponi, R. Osellame, and J. L. O'Brien, *Applied Physics Letters*, **100**, 233704+ (2012), ISSN 00036951.
- [5] E. Knill, R. Laflamme, and G. J. Milburn, *Nature*, **409**, 46 (2001), ISSN 0028-0836.
- [6] J. L. O'Brien, A. Furusawa, and J. Vuckovic, *Nature Photonics*, **3**, 687 (2009), ISSN 1749-4885.
- [7] P. J. Shadbolt, M. R. Verde, A. Peruzzo, A. Politi, A. Laing, M. Lobino, J. C. F. Matthews, M. G. Thompson, and J. L. O'Brien, *Nat Photon*, **6**, 45 (2012).
- [8] A. Peruzzo, M. Lobino, J. C. F. Matthews, N. Matsuda, A. Politi, K. Poullos, X.-Q. Zhou, Y. Lahini, N. Ismail, K. Wörhoff, Y. Bromberg, Y. Silberberg, M. G. Thompson, and J. L. O'Brien, *Science*, **329**, 1500 (2010), ISSN 1095-9203.
- [9] B. J. Metcalf, N. Thomas-Peter, J. B. Spring, D. Kundys, M. A. Broome, P. C. Humphreys, X.-M. Jin, M. Barbieri, W. S. Kolthammer, J. C. Gates, B. J. Smith, N. K. Langford, P. G. R. Smith, and I. A. Walmsley, *Nature Communications*, **4**, 1356 (2013).
- [10] J. E. Sharping, K. F. Lee, M. A. Foster, A. C. Turner, B. S. Schmidt, M. Lipson, A. L. Gaeta, and P. Kumar, *Opt. Express*, **14**, 12388 (2006).
- [11] S. Clemmen, K. P. Huy, W. Bogaerts, R. G. Baets, P. Emplit, and S. Massar, *Opt. Express*, **17**, 16558 (2009).
- [12] S. Azzini, D. Grassani, M. J. Strain, M. Sorel, L. G. Helt, J. E. Sipe, M. Liscidini, M. Galli, and D. Bajoni, *Opt. Express*, **20**, 23100 (2012).
- [13] S. Tanzilli, W. Tittel, H. De Riedmatten, H. Zbinden, P. Baldi, M. DeMicheli, D. B. Ostrowsky, N. Gisin, S. Tanzilli, W. Tittel, H. De Riedmatten, H. Zbinden, P. Baldi, M. DeMicheli, D. B. Ostrowsky, and N. Gisin, *The European Physical Journal D - Atomic, Molecular, Optical and Plasma Physics*, **18**, 155 (2002), ISSN 1434-6060.
- [14] W. H. P. Pernice, C. Schuck, O. Minaeva, M. Li, G. N. Goltsman, A. V. Sergienko, and H. X. Tang, *Nature Communications*, **3**, 1325 (2012).
- [15] A. Martin, O. Alibart, M. P. De Micheli, D. B. Ostrowsky, and S. Tanzilli, *New Journal of Physics*, **14**, 025002+ (2012), ISSN 1367-2630.
- [16] N. Matsuda, H. Le Jeannic, H. Fukuda, T. Tsuchizawa, W. J. Munro, K. Shimizu, K. Yamada, Y. Tokura, and H. Takesue, *Scientific Reports*, **2** (2012), ISSN 2045-2322, doi:10.1038/srep00817.
- [17] R. Soref, *Selected Topics in Quantum Electronics*, *IEEE Journal of*, **12**, 1678 (2006), ISSN 1077-260X.
- [18] J. Sun, E. Timurdogan, A. Yaacobi, E. S. Hosseini, and M. R. Watts, *Nature*, **493**, 195 (2013).
- [19] D. Bonneau, E. Engin, K. Ohira, N. Suzuki, H. Yoshida, N. Iizuka, M. Ezaki, C. M. Natarajan, M. G. Tanner, R. H. Hadfield, S. N. Dorenbos, V. Zwiller, J. L. O'Brien, and M. G. Thompson, *New Journal of Physics*, **14**, 045003+ (2012), ISSN 1367-2630.
- [20] H. Takesue, H. Fukuda, T. Tsuchizawa, T. Watanabe, K. Yamada, Y. Tokura, and S.-i. Itabashi, *Opt. Express*, **16**, 5721 (2008).
- [21] C. Xiong, C. Monat, A. Clark, C. Grillet, G. Marshall, M. Steel, J. Li, L. O'Faolain, T. Krauss, and J. Rarity, *Opt. Lett.*, **36**, 3413 (2011).
- [22] J. Chen, K. F. Lee, and P. Kumar, *Physical Review A*, **76**, 031804+ (2007).
- [23] J. C. F. Matthews, A. Politi, StefanovAndre, and J. L. O'Brien, *Nat Photon*, **3**, 346 (2009), ISSN 1749-4885.
- [24] S. Ramelow, L. Ratschbacher, A. Fedrizzi, N. K. Langford, and A. Zeilinger, *Physical Review Letters*, **103**, 253601+ (2009).
- [25] J. G. Rarity and P. R. Tapster, *Physical Review A*, **41**, 5139 (1990).
- [26] C. K. Hong, Z. Y. Ou, and L. Mandel, *Physical Review Letters*, **59**, 2044 (1987).
- [27] Z. Y. Ou and L. Mandel, *Physical Review Letters*, **61**, 54 (1988).
- [28] L. G. Helt, Z. Yang, M. Liscidini, and J. E. Sipe, *Opt. Lett.*, **35**, 3006 (2010).

- [29] A. Laing, A. Peruzzo, A. Politi, M. R. Verde, M. Halder, T. C. Ralph, M. G. Thompson, and J. L. O'Brien, *Applied Physics Letters*, **97**, 211109+ (2010).
- [30] X.-C. Yao, T.-X. Wang, P. Xu, H. Lu, G.-S. Pan, X.-H. Bao, C.-Z. Peng, C.-Y. Lu, Y.-A. Chen, and J.-W. Pan, *Nat Photon*, **6**, 225 (2012).
- [31] X.-C. Yao, T.-X. Wang, H.-Z. Chen, W.-B. Gao, A. G. Fowler, R. Raussendorf, Z.-B. Chen, N.-L. Liu, C.-Y. Lu, Y.-J. Deng, Y.-A. Chen, and J.-W. Pan, *Nature*, **482**, 489 (2012), ISSN 0028-0836.
- [32] S. Zotter, J. Kofler, T. Jennewein, and A. Zeilinger, *Physical Review A* (2011).
- [33] J. Mower and D. Englund, *Physical Review A*, **84**, 052326+ (2011).